The STAR Heavy Flavor Tracker (HFT): focus on the MAPS based PXL detector

Giacomo Contin[a,*], Eric Anderssen[a], Leo Greiner[a], Joachim Schambach[b], Joseph Silber[a], Thorsten Stezelberger[a], Xiangming Sun[c], Michal Szelezniak[d], Chinh Vu[a], Howard Wieman[a], Sam Woodmansee[a],

[a]*Lawrence Berkeley National Laboratory, Berkeley, CA 94720, USA*
[b]*University of Texas, 1 University Station, Austin, TX 78712, USA*
[c]*Central China Normal University (CCNU), Wuhan, China*
[d]*Institut Pluridisciplinaire Hubert Curien (IPHC), Strasbourg, France*

Abstract

The heavy quark hadrons are suggested as a clean probe for studying the early dynamic evolution of the dense and hot medium created in high-energy nuclear collisions. The Heavy Flavor Tracker (HFT) of the STAR experiment, designed to improve the vertex resolution and extend the measurement capabilities in the heavy flavor domain, was installed for the 2014 heavy ion run of RHIC.

It is composed of three different silicon detectors arranged in four concentric cylinders close to the STAR interaction point. The two inner-most layers are based on CMOS monolithic active pixels (MAPS), featured for the first time in a collider experiment, while the two outer layers are based on pads and strips. The two innermost HFT layers are placed at a radius of 2.7 and 8 cm from the beam line and accommodate 400 ultra-thin ($50\,\mu m$) high resolution MAPS sensors arranged in 10-sensor ladders to cover a total silicon area of $0.16\,m^2$. Each sensor includes a pixel array of 928 rows and 960 columns with a $20.7\,\mu m$ pixel pitch, providing a sensitive area of $\sim 3.8\,cm^2$. The sensor features $185.6\,\mu s$ readout time and $170\,mW/cm^2$ power dissipation. The detector is air-cooled, allowing a global material budget as low as $0.39\%\,X/X_0$ on the inner layer. A novel mechanical approach to detector insertion enables effective installation and integration of the pixel layers within an 8 hour shift during the on-going STAR run.

After a detailed description of the design specifications and the technology implementation, the detector status and operations during the current $200\,GeV$ Au+Au run will be presented in this paper, with a particular focus on calibration and general system operations aimed at stabilizing the running conditions. A preliminary estimation of the detector performance meeting the design requirements will be reported.

Keywords: MAPS, Pixel, Vertex, Probe testing, Insertion mechanics, Heavy Ions, HFT, STAR, RHIC

1. Physics Motivation and Detector Design

One of the main goals of the STAR experiment at the relativistic Heavy Ion Collider (RHIC) at the Brookhaven National Laboratory is to study p+p, d+Au, and Au+Au collisions at several energies up to $\sqrt{s} = 200\,GeV$ for A+A and up to $\sqrt{s} = 500\,GeV$ for p+p collisions with the aim to reproduce and characterize

the QCD phase transition between hadrons and partons. Heavy quark measurements are a key component of the heavy ion program for the systematic characterization of the dense medium created in heavy ion collisions, the so-called Quark-Gluon Plasma (QGP) [1]. Due to their mass, heavy quarks are only produced by hard processes early in the collision and not by thermal processes after the equilibration of the plasma, which makes mesons containing heavy quarks an ideal probe for studying the initial conditions of the produced QGP. The STAR experiment uses a Time Projection Chamber

*Corresponding author
Email address:* gcontin@lbl.gov (Giacomo Contin)

(TPC) inside a 0.5 T magnetic field as its main tracking detector. With its 1 mm pointing resolution, the TPC is not able to resolve the decay vertices of short-lived particles, like D^0 mesons (cτ=~120 μm). The Heavy Flavor Tracker (HFT) has been designed to extend the STAR measurement capabilities in the heavy flavor domain [2]. It consists of 4 cylindrical layers of silicon detectors inserted inside the TPC inner field cage. The outermost layer is placed at 22 cm from the beam line and is equipped with the Silicon Strip Detector (SSD): it is based on double sided silicon strip sensors with 95 μm interstrip pitch and 35 $mrad$ relative P- N-side stereo angle inclination; the SSD silicon and front-end chips come from an existing detector and have been equipped with new faster electronics. The Intermediate Silicon Tracker (IST) is placed at 14 cm radius and based on single-sided silicon pad sensors with 600 μm x 6 mm pitch. The two innermost layers, at 8 and 2.7 cm radius, feature MAPS PiXeL detectors (PXL) for the first time in a vertex detector at a collider experiment. STAR achieves the required DCA pointing resolution by tracking inward with graded resolution from the TPC (1 mm resolution) to the vertex, by using the SSD and IST (~250-300 μm) to guide tracks to the two innermost layers of PXL (~30 μm),

In order to achieve the required spatial resolution on the inner tracking hit points, the PXL detector uses state-of-the-art ultra thin CMOS Monolithic Active Pixel Sensors (MAPS) [3, 4, 5, 6] sensors with 20.7 μm x 20.7 μm pixel size, providing a single hit spatial resolution of 6 μm that can be improved to 3.6 μm through cluster centroid reconstruction methods. The sensors are thinned to 50 μm thickness to reduce multiple coulomb scattering. A relatively low power dissipation of 170 mW/cm^2 allows these sensors to be operated at room temperature with just air cooling, resulting in a further reduction of the material budget. The relatively short integration time (185.6 μs) and the radiation tolerance (up to 90 $kRad/year$ and $2 \cdot 10^{11}$ to 10^{12} $1MeV$ n_{eq}/cm^2) meet the requirements imposed by the STAR experimental conditions. In case of damage to the running detector, a novel approach to insertion mechanics allows replacing it with a spare detector copy within one day.

2. Design Implementation

The PXL detector features a highly parallel system architecture. It is subdivided into 2 detector-halves attached on one side to unique cantilevered mechanics, allowing for fast insertion and retraction of the detector by pushing the detector halves along rails inside a

support cylinder and locking them into a reproducible position with kinematic mounts. Each half consists of 5 sectors mounted in dovetail slots; a sector represents the basic unit in terms of powering and readout and consists of a trapezoidal thin (200 μm) carbon fiber sector tube with four 10-sensor ladders mounted on each tube, one at the inner diameter, and 3 at the outer diameter, arranged in a turbo geometry design (see Fig. 1). The sensors are thinned to 50 μm thickness, and are mounted on an aluminum conductor flex cable that provides the signal path to the electronics at the end of the flex cable containing the buffers and drivers for the sensor signals. This construction results in a total radiation length X/X_0 as little as 0.4% on the inner layer equipped with aluminum conductor flex cables.

The sensor chip used for the PXL detector is the *Ultimate-2* MAPS sensor developed by IPHC in Strasbourg, France, and optimized for the STAR environment. These sensors use pixels with a pitch of 20.7 μm arranged in a 928 (rows) by 960 (columns) array (a total of 890k pixels per sensor) on a 20.22 mm × 22.71 mm chip with a high-resistivity epitaxial layer for increased radiation hardness and improved signal-to-noise performance. Each pixel includes readout and correlated double sampling (CDS) circuitry for signal extraction and noise subtraction. The reticle is divided into 4 sub-arrays allowing for process variation compensation through the independent configuration of the reference voltages. The readout is done by reading each pixel row in parallel through programmable threshold discriminators at the end of each column. The resulting digital data are then passed through a zero-suppression logic block located at the periphery of the pixel array on the same chip, which delivers run-length encoded hit addresses for up to 9 hit clusters per row; the data is then passed to on-chip memory for intermediate buffering. The memory is arranged in two banks of 1500 words each which allows simultaneous read and write operations. The data are read out bit- serially from one of these memory banks over two Low-Voltage Differential Signaling (LVDS) outputs per sensor, each running at 160MHz. The integration time of the whole sensor is 185.6 μs. Configuration by the JTAG protocol allows the control of many internal parameters.

3. Detector Production

The PXL detector production started at the end of 2012 and was completed by the Fall of 2014. The production process consists of four subsequent phases: sensor probe testing, ladder assembly, sector assembly and
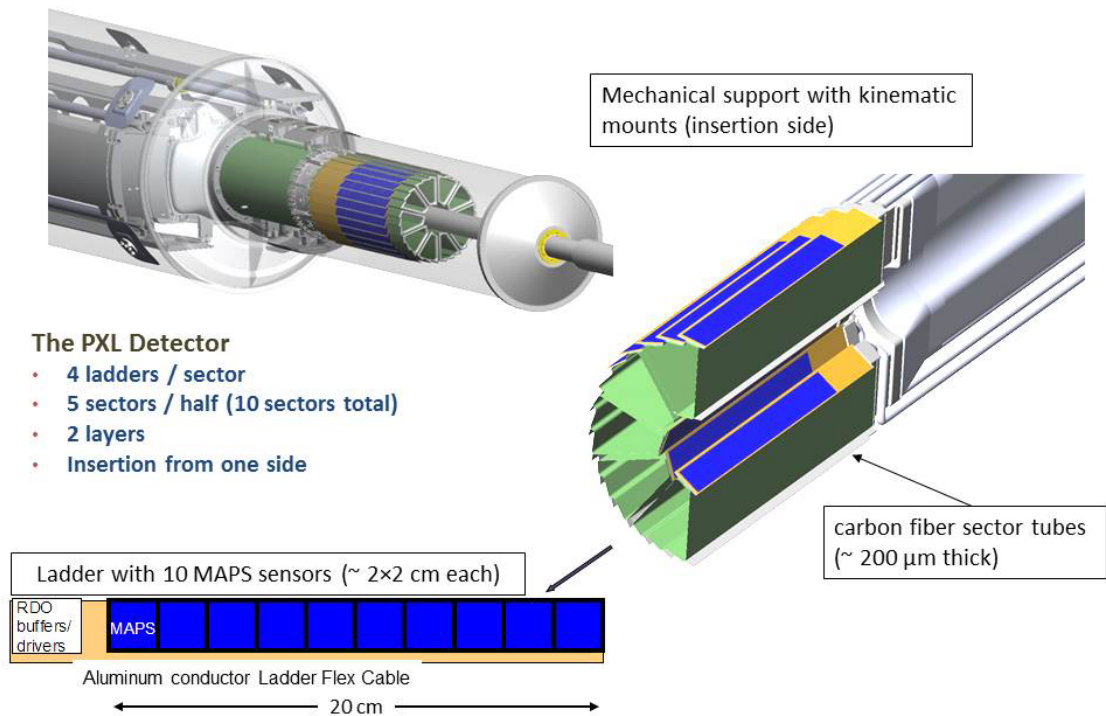
Figure 1: The PXL detector design.

detector half assembly. All the components are validated prior to assembly and the functionalities of the manufactured device are verified after each production step.

The thinned and diced sensors, typically curved due to their reduced thickness, are positioned on a custom made vacuum chuck and contacted through pins, which are mounted on a dedicated electronics probe card and designed to deal with the uneven pad ring surface: the sensor is tested for functional operation, fully characterized in terms of noise and operating thresholds through built-in test functionalities and the readout is tested at full speed (160 MHz). The yield of sensors within specifications ranged from 46% to 60% throughout the probe testing campaign.

Once selected, the sensors are manually positioned with butted edges on the ladder assembly fixtures and glued to the flex cable through an adhesive layer, preventing damages arising from different thermal expansion characteristics (see Fig. 2). The sensors and the front-end electronics are electrically connected via standard wire bonding to the flex cable and the wires are en-

capsulated for protection. The structure is stiffened by a carbon fiber backer glued at the bottom of the flex cable. Weights are taken at all assembly steps to track the material contributions and as QA; a series of reference pins and holes preserves the alignment of the different components throughout the ladder assembly procedure and the following sector assembly procedures.

At this point 4 ladders are glued on a carbon fiber sector tube in 4 steps to build a sector. Five sectors are finally mounted in dovetail slots on a detector half (see Fig. 3). All pixel positions on the sectors as well as the position of the sectors within a detector half are measured in a coordinate measurement machine (CMM). The ladder functionalities are tested after each assem-
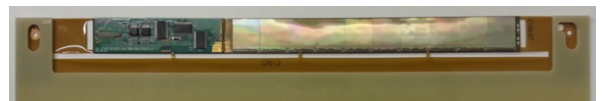

Figure 2: A PXL ladder: 10 sensors and the driver board glued on the flex cable, wire bonded and encapsulated.
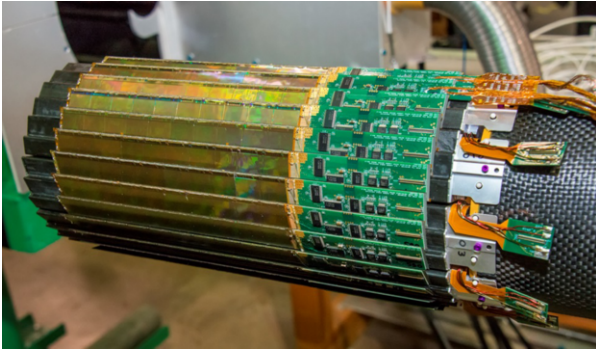
Figure 3: A PXL half-detector: 5 sectors mounted in dovetail slots on the carbon fiber support.

bly and position measurement step.

4. Detector Status, Operation and Performance

Two complete PXL detectors and 40 spare ladders have been fabricated by the fall of 2014 at the Lawrence Berkeley National Laboratory, in Berkeley, CA. The first detector copy, featuring 2 aluminum conductor and 8 copper conductor flex cables on the inner layer, was delivered to BNL at the end of 2013 and pre-commissioned through standalone runs in the STAR clean room; the copper conductor version of the flex cable results in a total radiation length X/X_0 lower than 0.5%, still meeting the minimal design requirements. The PXL detector was then inserted and cabled in the STAR TPC inner field cage and operational within 2 days. Before the 2014 heavy ion run, it was commissioned through STAR cosmic run data taking. During the cosmics run all 400 sensors of the PXL system were tested to be working properly with less than 2000 inactive pixels out of more than 365 million total. The pixel discriminator thresholds were adjusted to give a fake hit rate of $1.5 \cdot 10^{-6}$ for all sensors based on an automatic scan of noise rates versus discriminator threshold. The efficiency of the PXL detector was obtained from these data by finding cosmic ray tracks with hits on 3 PXL sensors, and looking for hits on a fourth sensor at the position of the extrapolated straight line through these three hits. Although this study was done before the detector operational parameter optimization was complete, the average efficiency over all sensors was determined to be 97.2%. This scan has been periodically repeated throughout the STAR 2014 run to take into account possible variations in the sensor response. Data from this cosmics run in absence of magnetic field were used for alignment studies of the PXL detector by finding cosmic ray tracks in the TPC with hits on 2 layers
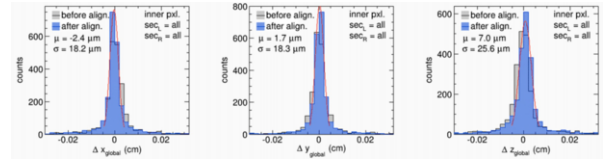

Figure 4: PXL hit residuals to cosmic tracks on the inner layer before and after PXL sector-to-sector alignment.

of a PXL detector half, and projecting the track to the inner and the outer layer of the other detector half.

After mapping the full detector half during construction as described above, the different parts of the PXL system were then aligned using these same cosmic ray data by looking at the residuals resulting from comparing hit positions to the track projections and adjusting the positions of the sensors in order to minimize these residuals. Gaussian fits to these residuals after the alignment was done result in a $\sigma \leq 25 \, \mu m$, which exceeds the PXL design goals (see Fig. 4).

The cosmic ray run was followed by a 4 week run period of Au+Au collisions at 14.5 GeV, used to optimize the sensor performance through discriminator threshold fine tuning. The next 17 weeks were devoted to 200 GeV Au+Au collisions during which a total of 1.2B minimum bias events with PXL included were recorded. Daily PXL noise runs without beam collisions were taken to reassess the sensor status, find inactive pixels, and to verify the noise levels. Periodic threshold-vs-noise scans were performed to readjust the discriminator thresholds. During the final ^{3}He+Au run of RHIC, PXL was only occasionally turned on for further performance and sensor damage studies.

During the 14.5 GeV Au+Au run and into the first two weeks of the 200 GeV Au+Au run sensor damage has been observed on the powered PXL detector. The damage took on many different forms: increased current in the digital power circuit, damaged or total loss of pixel columns, damaged configuration registers, loss of full or partial sub arrays, etc. Most of the damage occurred in the sensors of the innermost layer of PXL but even some sensors in the outer layer displayed these types of damage. It appears to be radiation related, possibly due to latch-up events: further damage to the installed detector was stopped for the rest of the run by reducing the over-current threshold closer to the normal operational current of the sensors, limiting in this way the energy released by the current excursion events. Other methods have been applied to protect the PXL detector from radiation damage: the sensors have been turned on when the collision rate started to fall below a
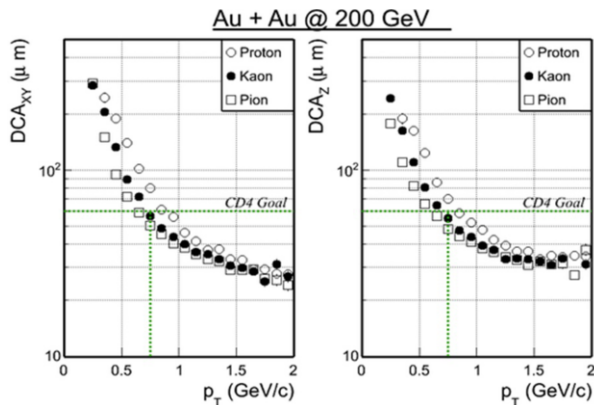
Figure 5: DCA resolution for TPC tracks with 1 IST hit and hits in both layers of PXL vs. transverse momentum.

certain threshold and reloading the sensor configuration periodically to reset. A total of 16 of the 400 sensors in the PXL detector were damaged, corresponding to a loss of 14% of the active surface on the innermost layer and 1% on the outer, but this still allowed for a successful completion of the 2014 physics run. These operational methods will be implemented from the beginning of the 2015 RHIC run, thus hopefully limiting damage to the PXL sensors in the future. The failure mechanism is now under extensive investigation by exposing existing PXL ladders and thinned sensors to heavy ion beam irradiation. This test is mainly aimed at characterizing the damage mechanism and at defining a safe operation envelope of LU current threshold settings for the 2015 run.

After the preliminary alignment corrections described above were completed, the 200 GeV data were used to estimate the pointing resolution of the PXL detector to the interaction vertex. The Distance of Closest Approach (DCA) resolution for tracks found in the TPC which include 1 IST hit and 1 hit in both layers of PXL as a function of transverse momentum p_T for protons, pions and kaons are shown in Fig. 5. For kaons with $p_T = 750\ MeV/c$ this DCA resolution exceeds the design goal of 60 μm, in fact, for p_T larger than 1.5 GeV/c, the DCA resolution is better than 30 μm. A more detailed determination of the alignment corrections is still ongoing which will further improve these results.

5. Conclusions

State-of-the-art MAPS technology has been used for the first time in a collider experiment for a vertex detector and demonstrated to be suitable for such application.

The STAR Heavy Flavor Tracker was installed, successfully integrated into STAR and commissioned for the 2014 Au+Au RHIC run. About 1.2 Billion (200 GeV Au+Au) events were taken to enable or enhance open heavy flavor measurements; 200 GeV p+p and more Au+Au data is expected to be taken in 2015 and 2016 RHIC runs. Preliminary studies demonstrate that the DCA pointing resolution performance of the installed detector meets the design goals. Sensor damage related to radiation has been observed. However, it was limited by applying operational methods during the run. The on-going latch-up mechanism investigation will provide the safe operation envelope of latch-up current threshold settings for the next RHIC runs. A second PXL detector equipped with aluminum flex cables on the inner ladders was constructed during the summer of 2014 and will be installed in STAR before the 2015 RHIC run. The damaged ladders during the 2014 RHIC run were replaced, and this detector will serve as a hot spare. A series of single spare ladders was also constructed and will be available should repairs be required in the future.

Acknowledgments

References

[1] J. Adams et al., Nucl. Phys. A, vol. 757, 102 (2005).
[2] D. Beavis et al., The STAR Heavy Flavor Tracker Technical Design Report, available at: https://drupal.star.bnl.gov/STAR/starnotes/public/sn0600 (2011)
[3] C. Hu-Guo, et al., Nucl. Instr. And Meth. A623 480 (2010).
[4] A. Dorokhov et al., Nucl. Instr. And Meth. A624 432 (2010).
[5] A. Dorokhov et al., Nucl. Instr. And Meth. A650 174 (2011).
[6] L. Greiner et al., Nucl. Instr. And Meth. A650 68 (2011).